Research Article | Vol. 9, No. 4 | 1 Apr 2018 | BIOMEDICAL OPTICS EXPRESS 1992

Biomedical Optics EXPRESS

Rapid volumetric imaging with Bessel-Beam three-photon microscopy

Bingying Chen,[1,7] Xiaoshuai Huang,[2,7] Dongzhou Gou,[2] Jianzhi Zeng,[3] Guoqing Chen,[2] Meijun Pang,[2] Yanhui Hu,[4] Zhe Zhao,[5] Yunfeng Zhang,[4] Zhuan Zhou,[2] Haitao Wu,[5] Heping Cheng,[2] Zhigang Zhang,[1] Chris Xu,[2,6] Yulong Li,[3] Liangyi Chen,[2,8] and Aimin Wang[1,9]

[1]*State Key Laboratory of Advanced Optical Communication System and Networks, School of Electronics Engineering and Computer Science, Peking University, Beijing 100871, China*
[2]*State Key Laboratory of Membrane Biology, Beijing Key Laboratory of Cardiometabolic Molecular Medicine, Institute of Molecular Medicine, Peking University, Beijing 100871, China*
[3]*State Key Laboratory of Membrane Biology, School of Life Sciences, PKU-IDG/McGovern Institute for Brain Research, Peking University, Beijing 100871, China*
[4]*School of Electronics Engineering and Computer Science, Peking University, Beijing 100871, China*
[5]*Department of Neurobiology, Institute of Basic Medical Sciences, Beijing, China*
[6]*School of Applied and Engineering Physics, Cornell University, Ithaca, NY 14853, USA*
[7]*These authors contributed equally to this work*
[8]*lychen@pku.edu.cn*
[9]*wangaimin@pku.edu.cn*

Abstract: Owing to its tissue-penetration ability, multi-photon fluorescence microscopy allows for the high-resolution, non-invasive imaging of deep tissue *in vivo*; the recently developed three-photon microscopy (3PM) has extended the depth of high-resolution, non-invasive functional imaging of mouse brains to beyond 1.0 mm. However, the low repetition rate of femtosecond lasers that are normally used in 3PM limits the temporal resolution of point-scanning three-photon microscopy. To increase the volumetric imaging speed of 3PM, we propose a combination of an axially elongated needle-like Bessel-beam with three-photon excitation (3PE) to image biological samples with an extended depth of focus. We demonstrate the higher signal-to-background ratio (SBR) of the Bessel-beam 3PM compared to the two-photon version both theoretically and experimentally. Finally, we perform simultaneous calcium imaging of brain regions at different axial locations in live fruit flies and rapid volumetric imaging of neuronal structures in live mouse brains. These results highlight the unique advantage of conducting rapid volumetric imaging with a high SBR in the deep brain *in vivo* using scanning Bessel-3PM.

© 2018 Optical Society of America under the terms of the OSA Open Access Publishing Agreement

OCIS codes: (110.0180) Microscopy; (180.2520) Fluorescence microscopy; (180.5810) Scanning microscopy; (190.4180) Multiphoton processes.

References and links

1. W. Denk, J. H. Strickler, and W. W. Webb, "Two-photon laser scanning fluorescence microscopy," Science **248**(4951), 73–76 (1990).
2. W. Denk and F. Helmchen, "Deep tissue two-photon microscopy," Nat. Methods **2**(12), 932–940 (2005).
3. W. R. Zipfel, R. M. Williams, and W. W. Webb, "Nonlinear magic: multiphoton microscopy in the biosciences," Nat. Biotechnol. **21**(11), 1369–1377 (2003).
4. D. Kobat, M. E. Durst, N. Nishimura, A. W. Wong, C. B. Schaffer, and C. Xu, "Deep tissue multiphoton microscopy using longer wavelength excitation," Opt. Express **17**(16), 13354–13364 (2009).
5. N. G. Horton, K. Wang, D. Kobat, C. G. Clark, F. W. Wise, C. B. Schaffer, and C. Xu, "*In vivo* three-photon microscopy of subcortical structure within an intact mouse brain," Nat. Photonics **7**(3), 205–209 (2013).
6. D. G. Ouzounov, T. Wang, M. Wang, D. D. Feng, N. G. Horton, J. C. C. Hernandez, Y. Cheng, J. Reimer, A. S. Tolias, N. Nishimura, and C. Xu, "*In vivo* three-photon imaging of activity of GCaMP6-labeled neurons deep in intact mouse brain," Nat. Methods **14**(4), 388–390 (2017).
7. L. Cheng, N. G. Horton, K. Wang, S. Chen, and C. Xu, "Measurements of multiphoton action cross sections for multiphoton microscopy," Biomed. Opt. Express **5**(10), 3427–3433 (2014).

#322760 https://doi.org/10.1364/BOE.9.001992
Journal © 2018 Received 9 Feb 2018; revised 22 Mar 2018; accepted 23 Mar 2018; published 29 Mar 2018

Biomedical Optics EXPRESS

8. E. J. Botcherby, R. Juskaitis, M. J. Booth, and T. Wilson, "An optical technique for remote focusing in microscopy," Opt. Commun. **281**(4), 880–887 (2008).
9. W. Yang, J. K. Miller, L. C. Reid, E. Pnevmatikakis, L. Paninski, R. Yuste, and D. S. Peterka, "Simultaneous multi-plane imaging of neural circuits," Neuron **89**(2), 269–284 (2016).
10. G. D. Reddy, K. Kelleher, R. Fink, and P. Saggau, "Three-dimensional random access multiphoton microscopy for fast functional imaging of neuronal activity," Nat. Neurosci. **11**(6), 713–720 (2008).
11. E. J. Botcherby, R. Juskaitis, and T. Wilson, "Scanning two photon fluorescence microscopy with extended depth of field," Opt. Commun. **268**(2), 253–260 (2006).
12. P. Dufour, M. Piché, Y. D. Koninck, and N. McCarthy, "Two-photon excitation fluorescence microscopy with a high depth of field using an axicon," Appl. Opt. **45**(36), 9245–9252 (2006).
13. G. Theriault, Y. D. Koninck, and N. McCarthy, "Extended depth of field microscopy for rapid volumetric two-photon imaging," Opt. Express **21**(8), 10095–10104 (2013).
14. R. Lu, W. Sun, Y. Liang, A. Kerlin, J. Bierfeld, J. D. Seelig, D. E. Wilson, B. Scholl, B. Mohar, M. Tanimoto, M. Koyama, D. Fitzpatrick, M. B. Orger, and N. Ji, "Video-rate volumetric functional imaging of the brain at synaptic resolution," Nat. Neurosci. **20**(4), 620–628 (2017).
15. B. Chen, T. Jiang, W. Zong, L. Chen, Z. Zhang, and A. Wang, "910nm femtosecond Nd-doped fiber laser for *in vivo* two-photon microscopic imaging," Opt. Express **24**(15), 16544–16549 (2016).
16. B. Chen, H. Rong, X. Huang, R. Wu, D. Wu, Y. Li, L. Feng, Z. Zhang, L. Chen, and A. Wang, "Robust hollow-fiber-pigtailed 930 nm femtosecond Nd:fiber laser for volumetric two-photon imaging," Opt. Express **25**(19), 22704–22709 (2017).
17. L. Liang, Y. Li, C. J. Potter, O. Yizhar, K. Deisseroth, R. W. Tsien, and L. Luo, "GABAergic projection neurons route selective olfactory inputs to specific higher-order neurons," Neuron **79**(5), 917–931 (2013).
18. M. Ng, R. D. Roorda, S. Q. Lima, B. V. Zemelman, P. Morcillo, and G. Miesenboeck, "Transmission of olfactory information between three populations of neurons in the antennal lobe of the fly," Neuron **36**(3), 463–474 (2002).
19. C. Xu and W. W. Webb, "Multiphoton Excitation of Molecular Fluorophores and Nonlinear Laser Microscopy," in *Topics in Fluorescence Spectroscopy*, J. R. Lakowiczv, ed. (Kluwer Academic Publishers, 1997).
20. O. Brzobohaty, T. Cizmar, and P. Zemanek, "High quality quasi-Bessel beam generated by round-tip axicon," Opt. Express **16**(17), 12688–12700 (2008).
21. R. F. Stocker, G. Heimbeck, N. Gendre, and J. S. Belle, "Neuroblast Ablation in *Drosophila* P[GAL4] Lines Reveals Origins of Olfactory Interneurons," J. Neurobiol. **32**(5), 443–456 (1997).
22. J. W. Wang, A. M. Wong, J. Flores, L. B. Vosshall, and R. Axel, "Two-Photon Calcium Imaging Reveals an Odor-Evoked Map of Activity in the Fly Brain," Cell **112**(2), 271–282 (2003).
23. J. B. Connolly, I. J. H. Roberts, J. D. Armstrong, K. Kaiser, M. Forte, T. Tully, and C. J. O'Kane, "Associative Learning Disrupted by Impaired Gs Signaling in *Drosophila* Mushroom Bodies," Science **274**(5295), 2104–2107 (1996).
24. M. Heisenberg, "Mushroom Body Memoir: From Maps to Models," Nature **4**(4), 266–275 (2003).

1. Introduction

Multi-photon microscopy (MPM) holds the promise of unique and impactful applications in cell biology and neuroscience research, where it can enable the high-resolution imaging of the neuronal structures buried deep inside the intact brain [1–3]. Benefiting from higher order nonlinear excitation and longer excitation wavelengths, 3PM has shown better performance in terms of the signal-to-background ratio (SBR) than has two-photon microscopy (2PM), and it has extended the non-invasive functional imaging of the mouse brain to beyond 1.0 mm. Using 3PM, the spontaneous activity recording in the hippocampal stratum pyramidale has been realized [4–6].

MPM normally uses focused femtosecond laser pulses to illuminate the sample, which limits the excitation volume to the focal point. Therefore, the sample must be imaged pixel by pixel to obtain a 3D image stack. In particular, the mechanical movement of the objective to perform the axial scanning decreases the imaging rate. This hampers its application in recording the activity of the large neuronal circuits distributed in a 3D volume. Moreover, the low repetition rate of femtosecond lasers (1-2 MHz) optimized for deep-tissue 3PE further limits the temporal resolution of point-scanning 3PM [7].

Various alternative axial scanning methods have been proposed to address this problem, such as fast z-scanning with remote focusing [8], wavefront shaping using spatial light modulators (SLM) [9], and random access scanning with acousto-optic deflectors (AOD) [10]. For sparsely labeled samples, using a Bessel beam to image a 3D volume is another feasible approach. The Bessel beam has an axially elongated, needle-like optical intensity

Biomedical Optics EXPRESS

distribution and maintains the same lateral resolution over an extended depth of field [11, 12]. Hence, a single scan can generate a 2D projection of the 3D volume image. Given that a single neuron often has dendrites that are sparsely distributed in a 3D volume, Bessel beam scanning is an excellent fast imaging method for obtaining volumetric information about the neuronal structures and activities. Moreover, the image obtained with Bessel-3PM is a 2D projection of a 3D object, which cannot offer the information in z-axis. Therefore, we can use Bessel-3PM to obtain the temporal information at different depths and use point-scanning 3PM to obtain the imaging depth as assistance. Nevertheless, the sample must be sparsely labeled; otherwise, this approach will cease to be effective if too much axial information is stacked together.

The Bessel beam has been used to extend the depth of field in 2PM of neurons [13, 14]. However, the intensity distribution of the zeroth-order Bessel beam in the transverse plane has strong side lobes under two-photon excitation (2PE) that generate an undesirable background and decrease the SBR. Because 3PE and 2PE fluorescence obey the cubic and quadratic dependence on the excitation power, respectively, a Bessel beam with 3PE has much smaller side lobes than does that with 2PE. In this paper, we compared the performance of 2PE and 3PE Bessel-beam using femtosecond lasers at 920 nm and 1300 nm, respectively, and demonstrate the superior SBR of volumetric Bessel 3PM in imaging zebrafish larva, fruit flies and mice *in vivo*.

2. Method and materials

2.1 Three- and two-photon imaging systems with Bessel-beam or Gaussian-beam excitation

A schematic diagram of the optical setup is shown in Fig. 1.

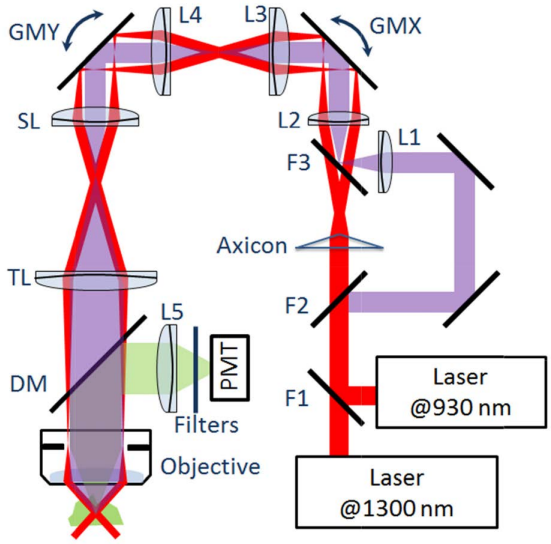

Fig. 1. Schematic diagram of the apparatus. Flipper mirrors: F1 was used to switch between 920 nm and 1300 nm lasers; F2 and F3 were used to switch between the Gaussian and Bessel beam excitation. Axicon, α = 2 degrees. Lenses: L1 and L2, 50 mm (or 75, 100 mm) focal length, determines the effective excitation NAs and lengths of the Bessel beam. L3 (100 mm), L4 (100 mm), SL (54 mm) and TL (200 mm) were used to create multiple conjugate planes of the back focal plane (BFP) of the objective in the light path; L5, collection lens (30 mm). Galvo mirrors: GMX/GMY, for the x/y direction of beam scanning. DM, 735-nm long-pass dichroic mirror; a 770-nm short pass filter and a 525/40 nm bandpass filter were used here (Filters) for emission collection.

Biomedical Optics EXPRESS

The light source for 3PM was a non-collinear optical parametric amplifier (NOPA, Spectra Physics) pumped by a 1040 nm high-power femtosecond laser (Spirit, Spectra Physics). The NOPA produced 50-fs pulses at 1300 nm with an average power over 500 mW and a repetition rate of 400 kHz. The femtosecond laser at 1300 nm could also be switched to a home-built femtosecond Nd:fiber laser, which delivered up to 800 mW, 150-fs pulses at 930 nm with a repetition rate of 50 MHz [15, 16]. This configuration enabled a comparison of the performance of 2PM and 3PM using the same specimen. After using a pair of scan mirrors (6215H, Cambridge Technology), the laser pulses were directed into a 54-mm scan lens and a 200-mm tube lens. A water immersion objective lens (XLPLN25XWMP2, 25X, NA 1.05, Olympus) was used to focus the light into the sample. The fluorescence emitted from the sample was epi-collected and directed to a GaAsP PMT detector (H7422p-40, Hamamatsu) by a long-pass dichroic mirror (FF735-Di02-25 × 36, Semrock). A collection lens, a short-pass filter (ET770sp-2p 1500IR, Chroma) and a 525/40 nm bandpass filter (FF02-525/40-25, Semrock) were used to collect the fluorescence signals. The microscope was compatible with two scanning modes: the Bessel-beam scanning mode and the point-scanning of Gaussian focal spot mode. For the Bessel-beam mode, a plano-convex axicon (1-APX-2-VIS-G254-P, Altechna) was used to generate the Bessel beam to excite the sample. The axial FWHM of Bessel beams depends on the different combinations of the angle α of the axicon (angle between the sloped and plane faces) and the focal length of Lens 2. For the point-scanning mode, lens L1 was used to collimate the beam before directing to the scan mirror. The transmission efficiencies through the system under both modes were approximately 25%.

The length of the Bessel-beam depends on optical components; however, for a certain biological experiment, the maximum extension is limited by the sample's property and the single pulse energy of the laser source. For tissues with high transparency, a long Bessel beam could be used to illuminate the entire imaging region (e.g. zebrafish). However, the length of the Bessel-beam should not be much longer than the thickness of the sample; otherwise, the excessive background fluorescence would be produced. Moreover, because of the limited excitation power, the beam length should be adjusted to even shorter to increase the imaging depth (e.g. mouse brain in our case). Hence, the appropriate length of depends on the sample's thickness and transparency, the depth of the imaging region, the single pulse energy of the laser source and other factors.

2.2 Sample preparation

In this work, three representative tissues (zebrafish, *Drosophila* and mouse brain) were used to characterize the properties of the imaging system.

The zebrafish was used to compare the SBR between 2PE and 3PE. The vascular epithelial cells were labeled with EGFP in the Tg (kdrl:EGFP) transgenic fish line. For imaging, the fish was raised in an embryo medium containing 0.002% phenylthiourea (PTU, Sigma) to suppress pigmentation synthesis. Prior to live imaging, the fish was anaesthetized with 0.01% tricaine (Sigma) to minimize the movement artifacts during imaging. Then, the anaesthetized zebrafish was embedded in a 1% ultra-pure agarose (Invitrogen) and immersed in E3 medium containing 0.01% tricaine.

For functional imaging, flies expressing GCaMP were reared at 25 °C on standard cornmeal for 8-12 days after eclosion before experiments. The procedures used for mounting and dissecting the flies for imaging were the same as previously described [17]. Flies were mounted to a small dish by tape, and the antennae were exposed to the air. The cuticle, fat bodies and air sacs between the eyes were removed to expose the brain. The exposed brains were perfused with adult-like hemolymph (ALH). Isoamyl acetate (IA, Sigma-Aldrich; Cat# 306967) was initially diluted by 100-fold in mineral oil (Sigma-Aldrich; Cat# 69794) (100 µl IA in 900 µl mineral oil) and then placed in a glass bottle. During olfactory stimulation, the airflow carrying IA (200 µl/min) was mixed with purified air (1000 ml/min) and delivered to the antennae of the flies. The identification of glomeruli was based on the map of the antenna

Biomedical Optics EXPRESS

lobe published previously [18]. The Fiji software was used to process the images of functional imaging experiments, including subtracting the background, smoothing with a Gaussian blur filter and measuring the fluorescence within the ROIs. The Origin software was used to process the raw data with binning and plot the traces. The pseudo-color snapshots (color-encoded by $\Delta F/F_0$) generated by Matlab with custom scripts were the averaged results of 2-4 repeats.

We used male C57BL/6J mice (20 g, 8 postnatal weeks, Thy-1-YFP) for *in vivo* brain imaging. Animals were prepared using the methods described in Ref [4]. The craniotomies were performed centered at 2.2 mm posterior and 3 mm lateral to the Bregma point. All procedures were approved by the Peking University Animal Use and Care Committee and complied with the standards of the Association for Assessment and Accreditation of Laboratory Animal Care, including the animal breeding and experimental manipulation.

3. Results and discussions

Following the analysis of Xu et al. [19], we can obtain the n-photon fluorescence:

$$\left\langle F(t)_n \right\rangle = \mathrm{C_n} I_0^n(t) \int d\boldsymbol{r} S^n(\boldsymbol{r}) \tag{1}$$

where $\mathrm{C_n}$ is a constant that depends on the dye concentration, the n-photon fluorescence cross-section, and the collection efficiency of the system. $I_0^n(t)$ and $S^n(\boldsymbol{r})$ are, respectively, the temporal and spatial intensity distributions of the excitation beam. Because the Bessel beam was transformed from a Gaussian beam by an axicon, $S(\boldsymbol{r})$ is given by [13]

$$S(r,z) = S_1(z) S_2(r) \tag{2}$$

$$S_1(z) = \frac{4\pi^2 \mathrm{NA}^2 z}{\lambda} exp(\frac{-2\mathrm{NA}^2 z^2}{w_0^2}) \tag{3}$$

$$S_2(r) = J_0^2(\frac{2\pi r \mathrm{NA}}{\lambda}) \tag{4}$$

where NA is the effective numerical aperture, λ is the wavelength of the laser, w_0 is the initial Gaussian beam width, and z, r and θ are the cylindrical coordinates. Using the equations above, the calculated point-spread functions (PSFs) in the x-z plane are shown in Fig. 2(a) (3PM) and Fig. 2(b) (2PM). The x-y intensity distributions after integrating the z-axis are shown in Fig. 2(e) (3PM) and Fig. 2(g) (2PM).

The total fluorescence of the m-th lobe for n-photon excitation can be calculated as

$$\left\langle F(t)_{nm} \right\rangle = \mathrm{C_n} I_0^n(t) \int S_1(z)^n dz \int_0^{2\pi} d\theta \int_{\frac{\lambda}{2\pi \mathrm{NA}} x_{m-1}^0}^{\frac{\lambda}{2\pi \mathrm{NA}} x_m^0} r S_2(r)^n dr \tag{5}$$

where x_m^0 is the m-th node (m > 0) of the zeroth order Bessel function, and x_0^0 is 0. From Eqs. (4) and (5), and with $\mathrm{r}' = \frac{2\pi r \mathrm{NA}}{\lambda}$, we obtain the ratio of fluorescence in the m-th lobe to fluorescence in the main lobe:

$$\frac{\left\langle F(t)_{nm} \right\rangle}{\left\langle F(t)_{n1} \right\rangle} = \frac{\int_{x_{m-1}^0}^{x_m^0} r' J_0^{2\mathrm{n}}(r') dr'}{\int_0^{x_1^0} r' J_0^{2\mathrm{n}}(r') dr'}. \tag{6}$$

Biomedical Optics EXPRESS

Equation (2) shows that the transverse distribution of the fluorescence generated by the Bessel beam is invariant along the z-axis, and Eq. (6) shows the relative fluorescence in the side lobes does not depend on the excitation NA, the length of the Bessel beam, or the pulse width. We define the fluorescence in the main lobe as the signal, and we define the rest, including the fluorescence in the side lobes and in regions far away from the focal area, as the background.

As shown in Fig. 2(e) and Fig. 2(g), the three-photon fluorescence in the 2nd lobe (i.e., m = 2) is approximately 5.3% that in the main lobe, while the two-photon fluorescence in the 2nd, 3rd and 4th lobes is approximately 27.2%, 15.2% and 10.6% that in the main lobe, respectively. The fluorescence generated by the side lobes of two-photon Bessel-beam significantly degrades the SBR of the image.

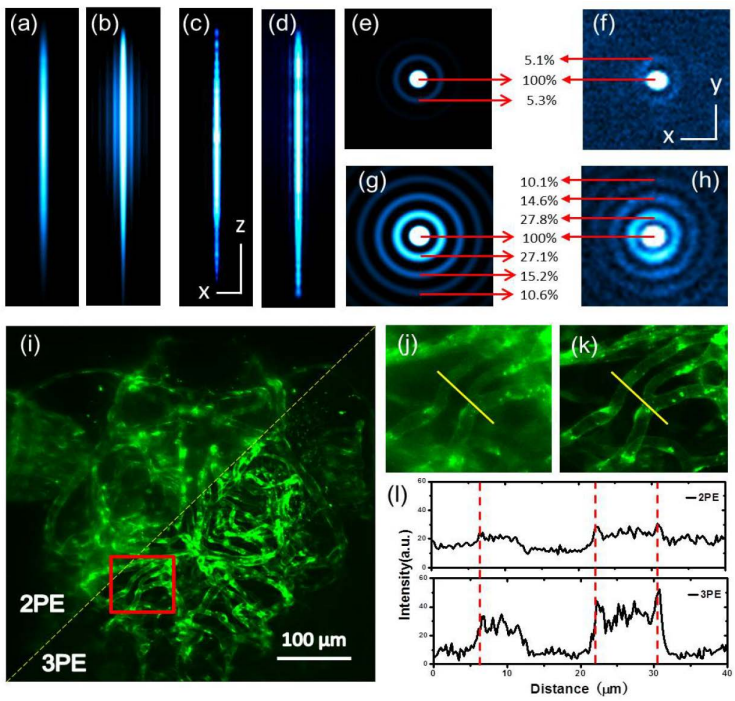

Fig. 2. Theoretically simulated and experimentally determined PSFs. (a)(b), simulated PSFs of 3PM and 2PM along the x-z planes. (c)(d), the experimental results. Scale bars, 100 µm (z), 2 µm (x). 0.5-µm fluorescent beads were used to measure xyz profiles of Bessel-3PM and Bessel-2PM. (e)(g), x-y cross section after integration of the z-axis of the Bessel beam to numerically simulate the fluorescence distribution of the side lobes (e, 3PM; g, 2PM), (f)(h), the experimental results. Scale bar, 2 µm. (i-l), comparison of blood vessels in live zebrafish imaged with Bessel-3PM and 2PM. (i), a representative example of the fish under Bessel 2PM and 3PM, in which the boxed region was magnified in j and k. (l), fluorescence intensities along the line across the same blood vessels.

We measured the lateral intensity distribution of fluorescent beads throughout the length of the Bessel beam for 2PE and 3PE. A stack of x-y images of 0.5-µm yellow/green (505/515) beads (Invitrogen) were recorded with a 2-µm depth increment using a constant excitation power. Figure 2(c), 2(d) show the axial PSFs of the Bessel beam of 3PM and 2PM. For focal length of L2 of 50 mm, the axial FWHMs of the Bessel beam were ~250 µm for 3PM and ~300 µm for 2PM. These values are in good agreement with theoretical predictions.

Biomedical Optics EXPRESS

The intensity modulation along the z-axis was caused by the round tip of the axicon [20]. Figures 2(f) and 2(h) show the x-y cross sections after integration of the z-axis of the Bessel beam using 3PE and 2PE. The lateral resolution (defined as the intensity FWHM) for 3PE and 2PE are approximately 0.7 µm and 0.6 µm, respectively, with an effective NA of 0.4. The lateral resolution can be improved with higher NA (e.g., 0.6 to 0.8). After the subtraction of the background, defined as the average pixel value from regions without fluorescent beads, the total fluorescence from all planes was integrated to estimate the side lobes, as shown in Fig. 2(f) and 2(h). The three-photon fluorescence of the 2nd lobe is 5.1% of the main lobe, and the two-photon fluorescence of the 2nd, 3th and 4th lobes are 27.8%, 14.6% and 10.1% of the main lobe, respectively, in good agreement with the calculated values. By integrating the fluorescence intensity from the first six side lobes, the combined fluorescence intensity of Bessel-3PM (8.7%) is less than one-eighth that of the Bessel-2PM (73.1%), indicating a much-improved SBR for Bessel-3PM.

We compared the performance of Bessel-3PM and Bessel-2PM in imaging blood vessels from a large volume (500 µm × 500 µm × 300 µm) in the same zebrafish (3 days post-fertilization) *in vivo*. We used the Tg (kdrl:EGFP) transgenic fish, in which EGFP was selectively expressed in vascular epithelial cells. The average power after the objective was 90 mW at 1300 nm for 3PM and 127 mW at 920 nm for 2PM. In agreement with the theoretical predictions and the experimental results with fluorescent beads, images obtained with Bessel-3PM were sharper than those obtained with Bessel-2PM [Fig. 2(i-l)].

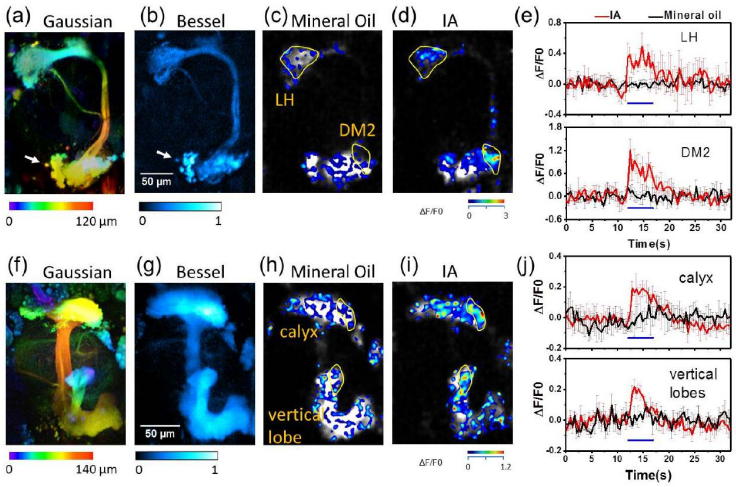

Fig. 3. Projection of volumetric imaging of GCaMP-labeled neuronal Ca^{2+} transients in olfactory centers of *Drosophila in vivo*. We stimulated the fly with isoamyl acetate (IA) for 5 s to trigger neuronal activities at the LH and the AL (DM2 glomerulus) of ePNs. (a), 3D neuronal structures under the point-scanning 3PM with color-coded by depth. (b), projection of 3D volume of neuronal structure under the Bessel-3PM. (c)(d), pseudo-color snapshots of the Ca^{2+} signals upon mineral oil and IA. (e), time-dependent Ca^{2+} responses from regions at the LH and the DM2 were recorded at a scanning rate of 5 Hz in experiments (c) and (d). Blue bar, stimulation duration. Individual traces are averaged results of 2-4 repeats and are processed with 2 × binning. Error bars, ± s.e.m. (f-j), similar experiments as (a)-(e), except that Kenyon cells at the MB were imaged. Axial FWHM of the Bessel beam, 110 µm. NA, 0.6.

Given the superior temporal resolution and comparative spatial resolution with point-scanning 3PM, we used the Bessel-3PM to monitor the fast dynamics of different olfactory centers of *Drosophila* along the axial direction *in vivo*. We genetically expressed GCaMP5 (GH146>GCaMP5 strain) [21] in the excitatory projection neurons (ePNs) at the antenna lobe (AL), where they relay crucial olfactory information from peripheral olfactory receptor neurons to higher brain centers, the mushroom body (MB) and the lateral horn (LH). The

application of odor isoamyl acetate (IA) could evoke calcium responses specifically in the DM2 glomerulus of the AL, as reported by point-scanning 2PM [22]. Figure 3(a) shows the 3D neuronal structure with depth coded by color under point-scanning 3PM. We acquired a 120-µm-deep stack taken at 2-µm depth increments, and each stack was averaged from 3 frames. Figure 3(b) shows the projective neuronal structure under Bessel-3PM (averaged from 10 frames). When imaging at the same frame rate (without averaging), point-scanning 3PM takes 60 times longer than Bessel-3PM. The small structures discernible in Fig. 3(a) and 3(b) (labeled by arrow) indicate the comparable spatial resolution for Bessel-3PM. Using Bessel-3PM, we simultaneously detected IA-evoked responses from discrete regions of the DM2 glomerulus and the LH at a frame rate of 5 Hz (256 × 256 pixels/frame). The application of the control mineral oil evoked no response [Fig. 3(c)], indicating the specificity of responses [Fig. 3(d)]. We also probed Ca^{2+} responses in Kenyon cells (KCs) at the MB (in OK107>GCaMP6s strain) [23], which are the third-order olfactory neurons thought to be critical for olfactory associative learning [24]. As shown in Fig. 3(f)-3(j), the amplitudes of IA-evoked Ca^{2+} responses from the calyx and the vertical lobe of the MB, which are 40 µm apart in axial distance, could be recorded simultaneously.

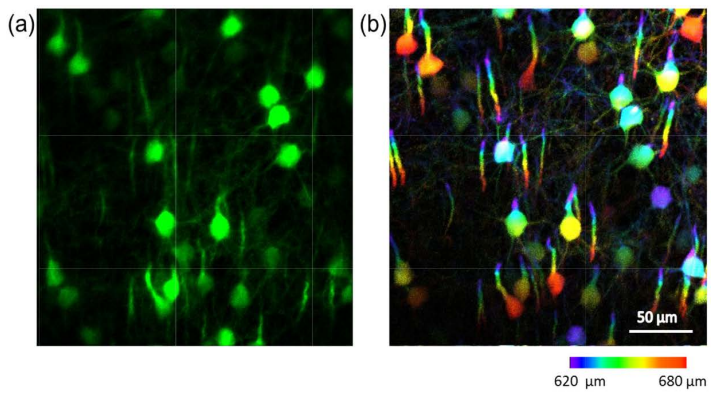

Fig. 4. *In vivo* three-photon images of neural cortex in a Thy1-YFP transgenic mouse. (a), projection of 3D volume neurons and neurites in cortex of the awake mouse taken with Bessel-beam at a frame rate of 1 Hz (image averaged from 10 frames afterwards). (b), mean intensity projection of a 65-µm-thick image stack collected at 1-µm z steps in point-scanning mode, from the same region as in (a). The stack covers from 620 µm to 685 µm below the dura, with structures color-coded by depth. The image of each layer was averaged from 3 frames, with a post objective power of 10 mW for Gaussian beam scanning and 110 mW for Bessel beam scanning.

Furthermore, we benchmarked the performance of Bessel-3PM to point-scanning 3PM in imaging 3D neuronal structures deeply buried in mice. We altered the focal length of L2 to 100 mm, which resulted in a 60 µm focal-depth Bessel beam for 3PM and an NA of 0.8. We used Bessel-beam scanning 3PM to image the brain of an awake mouse from 620 µm to 685 µm below the dura. The imaging speed was 1 Hz (512 × 512 pixels/frame) for a volume of 300 µm × 300 µm × 65 µm. Imaging the same volume with point-scanning 3PM required 1 min, which might contribute to the skewed structures due to motion artifacts (Fig. 4). These data highlights the importance and unique advantage of conducting rapid volumetric imaging in deep brain *in vivo* with scanning Bessel-3PM.

4. Summary

In this work, we presented the results of using a rapid volumetric 3PM method based on the axially elongated Bessel beam in imaging zebrafish larva, fruit flies and mice *in vivo*. The proposed method enables volume scanning as large as 500 µm × 500 µm × 300 µm at 5 Hz rate. Bessel-3PM has superior performance in terms of the penetration depth, SBR, and

Biomedical Optics EXPRESS

imaging speed and potentially provides a new multi-photon imaging tool to study the information processing within three-dimensional neural circuits *in vivo*.

Funding

The authors gratefully acknowledge funding from the National Natural Science Foundation of China (31327901, 61475008, 31428004, 31570839, and 31521062) and the National Science and Technology Major Project Program (2016YFA0500400).

Acknowledgment

The authors thank Hao Rong and Wan Yang for their help with the mechanical design. The Tg (kdrl:EGFP) fish was provided by Jingwei Xiong at Peking University.

Disclosures

The authors declare that there are no conflicts of interest related to this article.